

## Symmetry crossover in layered $MPS_3$ complexes ( $M=Mn, Fe, Ni$ ) via near-field infrared spectroscopy

S. N. Neal<sup>1</sup>, H.-S. Kim,<sup>2</sup> K. R. O'Neal<sup>1</sup>, A. V. Haglund<sup>3</sup>, K. A. Smith,<sup>1</sup> D. G. Mandrus,<sup>3,4</sup> H. A. Bechtel<sup>5</sup>, G. L. Carr,<sup>6</sup> K. Haule,<sup>2</sup> David Vanderbilt<sup>6,2</sup> and J. L. Musfeldt<sup>6,1,7,\*</sup>

<sup>1</sup>Department of Chemistry, University of Tennessee, Knoxville, Tennessee 37996, USA

<sup>2</sup>Department of Physics and Astronomy, Rutgers University, Piscataway, New Jersey 08854, USA

<sup>3</sup>Department of Materials Science and Engineering, University of Tennessee, Knoxville, Tennessee 37996, USA

<sup>4</sup>Materials Science and Technology Division, Oak Ridge National Laboratory, Oak Ridge, Tennessee 37831, USA

<sup>5</sup>Advanced Light Source Division, Lawrence Berkeley National Laboratory, Berkeley, California 94720, USA

<sup>6</sup>National Synchrotron Light Source II, Brookhaven National Laboratory, Upton, New York 11973, USA

<sup>7</sup>Department of Physics and Astronomy, University of Tennessee, Knoxville, Tennessee 37996, USA

(Received 3 May 2020; revised 16 July 2020; accepted 17 July 2020; published 6 August 2020)

We employ synchrotron-based near-field infrared spectroscopy to reveal the vibrational properties of bulk, few-sheet, and single-sheet members of the  $MPS_3$  ( $M=Mn, Fe, Ni$ ) family of materials and compare our findings with complementary lattice dynamics calculations.  $MnPS_3$  and the Fe analog are similar in terms of their symmetry crossovers, from  $C2/m$  to  $P\bar{3}1m$ , as the monolayer is approached. These states differ as to the presence of a  $C_3$  rotation around the metal center. On the other hand,  $NiPS_3$  does not show a symmetry crossover, and the lack of a  $B_u$  symmetry mode near  $450\text{ cm}^{-1}$  suggests that  $C_3$  rotational symmetry is already present, even in the bulk material. We discuss these findings in terms of local symmetry and temperature effects as well as the curious relationship between these symmetry transformations and those that take place under pressure.

DOI: [10.1103/PhysRevB.102.085408](https://doi.org/10.1103/PhysRevB.102.085408)

### I. INTRODUCTION

Complex chalcogenides like  $CrSiTe_3$ ,  $CrI_3$ , and  $CuInP_2S_6$  are superb platforms for revealing the interplay between charge, structure, and magnetism and unusual states of matter that develop under external stimuli [1–4]. These van der Waals solids can be exfoliated into few- and single-layer sheets that sport a number of unexpected properties, including quantum confinement, magnetic excitations and size-induced magnetic states, and symmetry breaking [5–13]. The  $MPS_3$  ( $M=Mn, Fe, Ni$ ) family of materials attracted our attention in this regard. These compounds are well suited to the development of structure-property relations, and the connection between few- and single-layer properties and those accessible under external stimuli are highly underexplored.

The  $MPS_3$  ( $M=Mn, Fe, Ni$ ) materials are thought to exist in the monoclinic space group  $C2/m$  [14–16]. Substitution of the metal center systematically alters the sheet thickness and van der Waals gap [Fig. 1(a)] as well as various bond lengths and angles [16,17].  $MnPS_3$  is a demonstrated linear magnetoelectric in the low-temperature phase [18]. Spectroscopy is unlocking properties suitable for optoelectronics applications [19,20], and external stimuli reveal layer sliding, superconductivity, piezochromism, and driven magnetic states, to name just a few [2,21–26]. The properties of these materials also evolve under exfoliation. Raman scattering, which measures the behavior of even-symmetry (*gerade*) modes, is regularly employed to study few- and single-sheet materials,

determining the number of layers, symmetry breaking, and electron-phonon coupling and even uncovering the suppression of magnetic order at the monolayer in  $NiPS_3$  [13,27,28]. Infrared spectroscopy is also a superb probe of local symmetry, revealing the behavior of odd-symmetry (*ungerade*) vibrational modes. It is, however, nearly impossible to apply

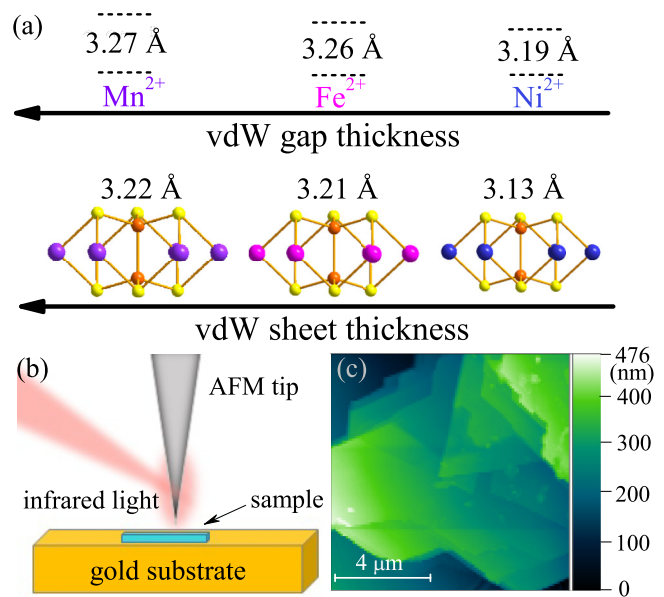


FIG. 1. (a) Van der Waals gap size and sheet thickness as a function of metal-site substitution. (b) Schematic of an AFM cantilever tip directing light to the sample surface. (c) High-resolution AFM image of few-layer  $FePS_3$ .

\*musfeldt@utk.edu

traditional infrared techniques to an exfoliated sample because (i) long-wavelength far-infrared light has a diffraction-limited focal point [29,30] and (ii) large-area thin films [31–34] are not currently available for every complex chalcogenide of interest. The ultrathin limit of  $\text{MnPS}_3$  is particularly notable for retention of magnetoelectric character [20].

Near-field infrared nanospectroscopy offers an important path forward. This technique combines a high-brightness, broadband light source, such as a synchrotron, with a Fourier transform infrared spectrometer and an atomic force microscope. In addition to imaging sheet topography, the tip focuses infrared light onto the sample with a  $20 \times 20 \text{ nm}^2$  spatial resolution [Figs. 1(b) and 1(c)], sufficient for work on few- and single-layer sheets, domain walls, and plasmons [35–37]. Our team recently employed this technique to reveal a  $C2/m \rightarrow P\bar{3}1m$  symmetry crossover in  $\text{MnPS}_3$  as a function of sheet thickness [36]. Symmetry is higher in the monolayer due to a restoration of the threefold rotation about the metal center. The availability of materials with different metal centers offers an opportunity to unravel structure-property relationships involving sheet thickness, symmetry, and local structure.

In order to explore symmetry effects in an important class of magnetic chalcogenides, we employed synchrotron-based near-field infrared spectroscopy to measure local lattice distortions in the  $\text{MPS}_3$  ( $M=\text{Mn, Fe, Ni}$ ) family of materials in bulk, few-layer, and single-layer forms. Analysis of the odd-symmetry vibrational modes reveals that the  $B_u$  feature near  $450 \text{ cm}^{-1}$  is exceptionally sensitive to the presence (or absence) of the  $C_3$  rotation about the metal center. Using this feature as a guide, we find that both  $\text{MnPS}_3$  and the Fe analog display a  $C2/m$  to  $P\bar{3}1m$  transition with decreasing thickness, whereas the third system,  $\text{NiPS}_3$ , retains its “ $C_3$ -ness” over the full range of sheet thicknesses. As a result, the structure of  $\text{NiPS}_3$  is  $P\bar{3}1m$ , even in the bulk. These findings are discussed in terms of the local structure, the stacking pattern, and temperature effects as well as slab thickness and van der Waals gap trends. Remarkably, the  $C2/m$  and  $P\bar{3}1m$  space groups preferred by  $\text{MnPS}_3$  for different layer numbers are identical to those observed under compression [25]. Here, the symmetry crossovers are triggered by pressure-induced layer sliding and a pressure-driven insulator-metal transition rather than a particular layer number. This suggests that symmetry-driven properties in few- and single-layer analogs can be accessed under pressure and strain as well.

## II. METHODS

Single crystals of  $\text{MnPS}_3$ ,  $\text{FePS}_3$ , and  $\text{NiPS}_3$  were grown using the chemical vapor transport process as described previously [38]. For near-field work, these crystals were mechanically exfoliated using thermal release tape and applied to the surface of a gold mirror. For far-field studies, a pinhole was used to support crystals with appropriate optical density. Near-field infrared nanospectroscopy was performed using Beamline 2.4 at the Advanced Light Source, Lawrence Berkeley National Laboratory. This setup consists of a commercial nanoscope (neaspec neaSNOM) coupled to a Cu:Ge detector and a silicon beam splitter [39]. Amplitude and phase were collected over the frequency range of  $330\text{--}700 \text{ cm}^{-1}$  and with a tip-limited spatial resolution on the order of  $20 \times 20 \text{ nm}^2$ . All near-field spectra employ second-harmonic signals (yield-

ing increased sensitivity) that contain the near-field response. For comparison, we measured traditional infrared absorption and Raman scattering using a Bruker 113v spectrometer equipped with a bolometer ( $20\text{--}700 \text{ cm}^{-1}$ ,  $2\text{-cm}^{-1}$  resolution) and a Horiba LabRAM HR Evolution spectrometer ( $50\text{--}700 \text{ cm}^{-1}$ ,  $\lambda_{\text{ex}} = 532 \text{ nm}$  at a power of  $0.5 \text{ mW}$  with an  $1800 \text{ line/mm}$  grating.)

*Ab initio* density functional theory (DFT) calculations were completed via the Vienna Ab initio Simulation Package (VASP), which employs the projector augmented-wave basis set [40,41]. For the treatment of electron correlations within DFT, a revised Perdew-Burke-Ernzerhof exchange-correlation functional for crystalline solids (PBEsol) was employed [42], augmented by on-site Coulomb interactions for transition-metal  $d$  orbitals within a simplified rotationally invariant form of the DFT +  $U_{\text{eff}}$  formalism [43]. Structural optimizations employed force criteria below  $10^{-4} \text{ eV/\AA}$ . PHONOPY code interfaced with VASP was employed to calculate the  $\Gamma$ -point phonon mode frequencies for each structure [44].

## III. RESULTS AND DISCUSSION

### A. Synchrotron-based near-field response of the $\text{MPS}_3$ family of materials ( $M=\text{Mn, Fe, Ni}$ )

Figure 2 summarizes the near-field spectra for the full set of  $\text{MPS}_3$  materials ( $M=\text{Mn, Fe, Ni}$ ). Both amplitude

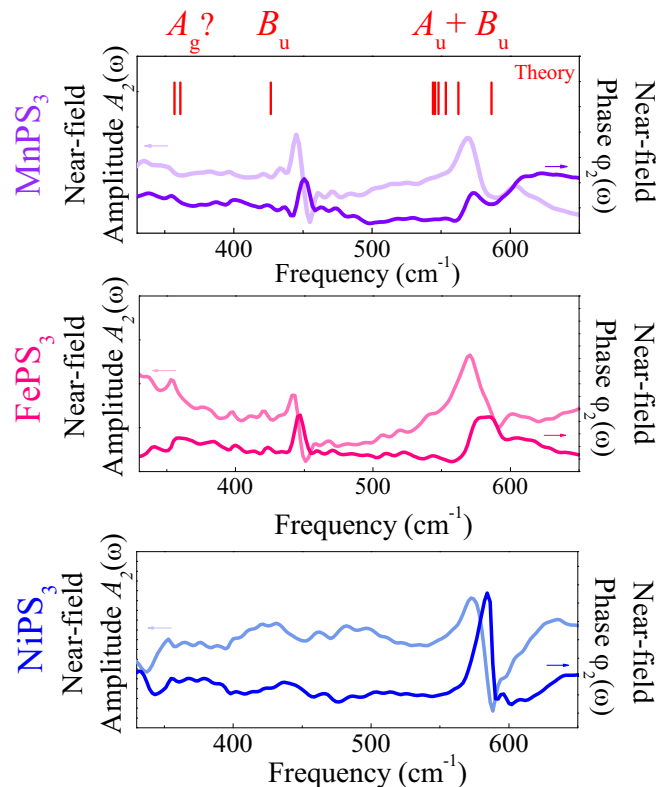


FIG. 2. Near-field amplitude and phase spectra for  $\text{MnPS}_3$ ,  $\text{FePS}_3$ , and  $\text{NiPS}_3$  single crystals at room temperature. Calculated mode positions and assignments are shown in the top panel. The overall scale focuses on the currently available near-field frequency window ( $330\text{--}650 \text{ cm}^{-1}$ ) of interest.

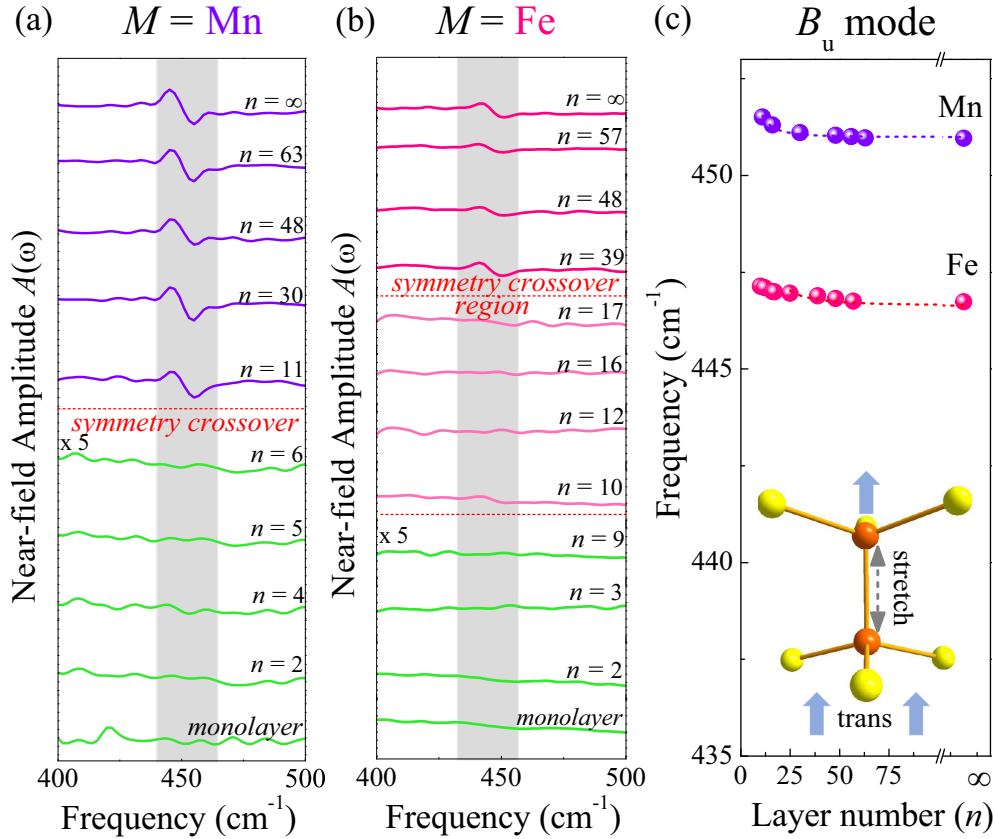


FIG. 3. (a) and (b) Close-up view of the near-field infrared response highlighting the behavior of the  $B_u$  symmetry vibrational mode in the  $M = Mn$  and Fe materials. Below  $n = 11$  (Mn) and  $n = 10$  (Fe), the data are multiplied by a factor of 5. The symmetry crossover is indicated, below which the  $B_u$  symmetry feature disappears. (c) Frequency vs layer number trends for the  $M = Mn$  and Fe compounds showing how the  $B_u$  symmetry mode hardens on the approach to the symmetry crossover. The dotted lines are a  $1/\text{size}^2$  fit to the data points. The model is discussed in the Supplemental Material. Error bars are smaller than the symbol size. A schematic view of the displacement pattern of the  $B_u$  symmetry vibrational mode is also included. The motion is a P-P stretch combined with in-phase, out-of-plane  $PS_3$  translation.

and phase signals are included to illustrate how this method works on single crystals and, at the same time, to provide the  $n = \infty$  response. Here,  $n$  is the layer number. Vibrational mode assignments are made via comparison with traditional infrared and Raman scattering spectra (see the Supplemental Material [45]) as well as prior lattice dynamics calculations of  $MnPS_3$  [36]. The high-frequency doublet structure, centered near  $567\text{ cm}^{-1}$  (Mn),  $580\text{ cm}^{-1}$  (Fe), and  $584\text{ cm}^{-1}$  (Ni), is assigned to the infrared active  $A_u + B_u$  modes, with an isotopelike effect evident in the frequency progression. The  $B_u$  mode near  $450\text{ cm}^{-1}$  is also present in the near-field spectrum of the Mn and Fe materials and significantly amplified compared to the far-field infrared response. This feature is absent in  $NiPS_3$  (Fig. S2). The amplified intensity of this structure in  $MnPS_3$  and  $FePS_3$  as well as its absence in the Ni analog will be important in our discussion below. The  $365\text{ cm}^{-1}$  feature in  $MnPS_3$  is tentatively assigned as an  $A_g$  symmetry mode, activated by the tip-enhanced nature of the near-field technique [36]. The relaxation of traditional selection rules can be attributed to the presence of highly concentrated and slightly curved electric field lines that manifest because of the way in which the evanescent wave travels down the tip to focus light on the sample. A similar structure is observed near  $357\text{ cm}^{-1}$  in  $FePS_3$ . A complete set of mode assignments, a

close-up view of the  $B_u$  vibrational mode in the single crystals, and a brief discussion of signal-to-noise considerations are available in the Supplemental Material [45].

### B. Using the $B_u$ symmetry vibrational mode to reveal symmetry crossovers

Figure 3 displays a close-up view of the near-field infrared response of  $MnPS_3$  and  $FePS_3$ , focusing on the behavior of the  $B_u$  vibrational mode. The displacement pattern of this odd-symmetry (ungerade) mode is a P-P stretch combined with in-phase, out-of-plane  $PS_3$  translation. This feature is very prominent in the spectrum of the  $MnPS_3$  and  $FePS_3$  single crystals. The amplification is probably due to the tip-enhanced nature of the near-field technique. The  $B_u$  symmetry vibrational mode is strong and well resolved in few-layer  $MnPS_3$  as well, shifting to higher frequency with decreasing layer number, consistent with expectations for confinement. Importantly, the  $B_u$  mode disappears below  $n = 11$ , indicative of a symmetry crossover in which the  $C_3$  rotation is restored [36]. In other words, the  $C2/m$  space group characterizes the  $MnPS_3$  single crystal as well as the few-layer system down to approximately  $n = 11$ . At smaller  $n$ , the signature of the  $B_u$  mode is lost—evidence of a transition to a

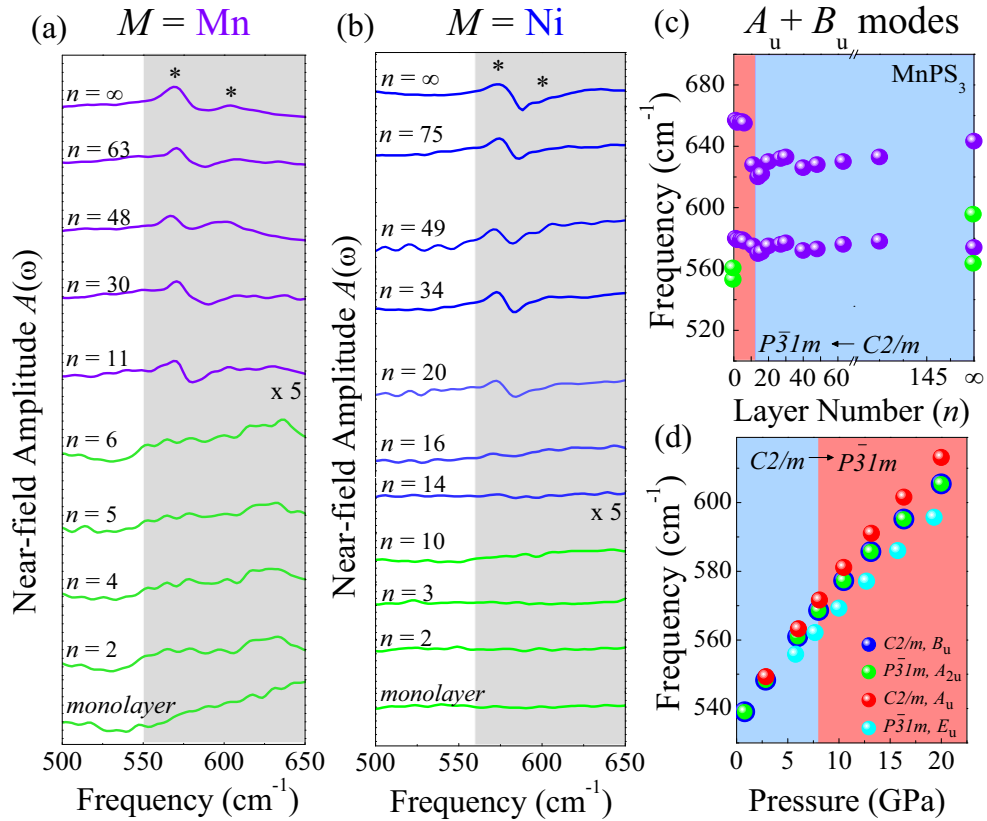


FIG. 4. Close-up view of the near-field infrared response in the region of the  $A_u + B_u$  modes for the (a) Mn and (b) Ni materials at 300 K. The symmetry crossover is indicated by the change in color (violet or blue to green). (c) Frequency vs layer number trend for MnPS<sub>3</sub> across the  $C2/m \rightarrow P\bar{3}1m$  transition for both experiment (violet) and theory (green). Error bars are smaller than the symbol size. (d) Theoretically predicted frequency shift of MnPS<sub>3</sub> across the pressure-induced  $C2/m \rightarrow P\bar{3}1m$  sliding transition. Inflection points are observed at the symmetry crossovers.

higher-symmetry state [Fig. 3(a)]. A correlation group analysis and first-principles modeling of the pattern of excitations reveal that the higher-symmetry space group at small  $n$  and in the monolayer is  $P\bar{3}1m$ . Temperature effects may be partially responsible for the restoration of the  $C_3$  rotation, although as we discuss below, crossovers between  $C2/m$  and  $P\bar{3}1m$  are seen in other contexts. Pressure is a prominent example.

Because the  $B_u$  mode is such a sensitive indicator of symmetry, we extended this analysis to other members of the  $MPS_3$  family with the goal of developing structure-property relationships. As shown in Fig. 3(b), the behavior of the  $B_u$  mode in FePS<sub>3</sub> is different than that in the Mn analog. As before, the  $B_u$  mode is strong and well defined in the large- $n$  regime. This system reveals a gradual crossover to the high-symmetry state. For instance, the  $B_u$  feature seemingly disappears after  $n = 17$ , only to reappear below  $n = 12$ . Thus, the symmetry crossover seems to take place across a region rather than at a specific layer number, as is the case for MnPS<sub>3</sub>. However, we still find the same  $C2/m \rightarrow P\bar{3}1m$  symmetry increase on approach to the monolayer. It is tempting to classify the symmetry crossover in MnPS<sub>3</sub> as a first-order transition and that in the Fe analog as a second-order transition. At this time, it is difficult to determine whether these symmetry crossovers are true thermodynamics transitions—verifiable by specific heat—or whether the difference is due to structural

flexibility and temperature effects. One consequence of a gradual transition in FePS<sub>3</sub> is the presence of a mixed phase between  $n = 17$  and 10.

Figure 3(c) shows frequency vs layer number trends for the  $B_u$  mode. We find overall blueshifts between 1 and 1.5 cm<sup>-1</sup>. Since frequency goes as  $\sqrt{\frac{k}{\mu}}$ , we can use the frequency shift in the  $B_u$  vibrational mode to estimate how the force constant changes with decreasing layer number. Here,  $k$  is the force constant, and  $\mu$  is the effective mass. We find that the force constant increases by approximately 1.0% in the single-sheet limit compared to that in the bulk. Although at the limit of our sensitivity, the Mn system appears to be fairly rigid until the symmetry crossover is approached, whereas the Fe analog shifts more gradually with decreasing layer number [Fig. 3(c)]. Fits to  $1/\text{size}^2$  are indicative of traditional quantum confinement, and the larger prefactor in MnPS<sub>3</sub> is consistent with greater stiffness. This model is discussed in detail in the Supplemental Material.

### C. $A_u + B_u$ sulfur-phosphorous stretching modes as a function of layer number

Figure 4 summarizes the near-field infrared response of the  $A_u + B_u$  sulfur-phosphorous stretching modes for both the Mn and Ni members of the  $MPS_3$  family as a function of

layer number. In each case, the  $n = \infty$  spectra evolve with decreasing thickness, always sporting a clear doublet pattern in this frequency regime. The doublet structure is denoted by asterisks [Figs. 4(a) and 4(b)]. In  $MnPS_3$ , the low-frequency branch of the doublet redshifts with decreasing thickness, whereas the high-frequency branch blueshifts slightly. There is significant broadening between  $n = 28$  and 22. Between  $n = 16$  and 11, the two branches come together slightly and begin to diminish. This change in spectral features is attributed to the symmetry crossover [36]. Below  $n = 11$ , the features broaden dramatically and upshift slightly as the monolayer is approached. Eventually (when  $n = 1$ ), the doublet structure that is the signature of the  $A_u + B_u$  modes is overcome by the gold- $\cdots$ sulfur charge transfer band [46] above  $550\text{ cm}^{-1}$  and cannot be resolved. Our lattice dynamics calculations reveal that there are a number of sulfur-phosphorous-related stretching modes that underlie the strong doublet pattern in this frequency region [36]. Plotting peak position vs layer number, we see that both structures soften with decreasing  $n$  in the  $C2/m$  phase, consistent with the notion that reducing interlayer interactions tends to soften a resonance [Fig. 4(c)]. We find, however, that both features show a marked upturn across the  $C2/m \rightarrow P\bar{3}1m$  transition.

The strong doublet structure that is characteristic of the  $A_u + B_u$  sulfur-phosphorous stretching modes is clearly recognizable in  $NiPS_3$  as well. It remains well resolved until  $n = 16$ , below which it becomes much less intense and then starts to broaden below  $n = 14$ . This doublet structure is, however, clearly retained at small  $n$ , suggesting that no symmetry crossover occurs in this material. The significantly smaller van der Waals gap and sheet thickness is anticipated to make  $NiPS_3$  less vulnerable to temperature and strain effects than the Mn and Fe analogs. Interestingly, the Au- $\cdots$ S charge transfer band [46] present in the Mn and Fe (not shown) analogs is absent in the near-field infrared spectrum of the  $NiPS_3$  monolayer.

#### D. Developing structure-property relations

Bringing these trends together, we find that monoclinicity in the  $MPS_3$  family of materials is the result of long-range stacking, temperature effects, and local structure. In other words, interslab proximity and thermally induced structural fluctuations work to restore the  $C_3$  rotation in small  $n$  members of the  $MPS_3$  series for  $M = Mn$  and  $Fe$  [47]. Thus,  $P\bar{3}1m$  symmetry prevails in few-layer sheets of  $MnPS_3$  and  $FePS_3$  as well as the monolayers. Interestingly, the  $n$  dependence of the  $C2/m$  to  $P\bar{3}1m$  symmetry crossover is not related to slab thickness or van der Waals gap in a straightforward manner.

On the other hand, if we consider thicker two-dimensional layers and larger van der Waals gaps to be associated with changes in chemical bonding and weaker interslab proximity effects, we can develop some loose structure-property relationships. For instance, the van der Waals gap in  $NiPS_3$  is the smallest of the series [Fig. 1(a)], so we expect interlayer interactions to be the strongest. Proximity effects from adjacent layers may therefore constrain the Ni compound to the high-symmetry  $P\bar{3}1m$  state over the full  $n$  range. This supposition is consistent with the total absence of the  $B_u$  symmetry vibrational mode in the near-field infrared response of  $NiPS_3$

(Fig. S2). This higher-order space group is in contrast to prior x-ray diffraction work [48–50], although because  $C2/m$  is a subgroup of  $P\bar{3}1m$ , they can have nearly indistinguishable diffraction patterns. More comprehensive efforts emphasize the importance of using a single crystal for structural determinations [51]. Both x-ray and neutron studies seem to reveal that these systems exist in  $C2/m$ , although there are significant discrepancies, including the observation of a (010) magnetic Bragg peak and extra peaks in the Laue diffraction that can be indexed only if  $C$  centering is removed [51]. Clearly, the quality of refinement and modeling is not ideal, suggesting the possibility of very subtle symmetry effects in  $NiPS_3$  compared to other members of the series. Moreover, the van der Waals gap in  $MnPS_3$  and  $FePS_3$  is significantly larger, which may provide additional flexibility as well as greater sensitivity to temperature. This picture is consistent with the discovery of pressure-induced sliding in  $FePS_3$  [22], which also benefits from a larger van der Waals distance and weaker interlayer interactions.

At the same time, the  $MPS_3$  series has well-known trends in sheet thickness [Fig. 1(a)]. The Mn and Fe compounds are nearly the same macroscopically (as indicated by their sheet thicknesses and van der Waals gaps) but not microscopically (in terms of their bond lengths and angles), whereas  $NiPS_3$  has an overall contraction of the lattice compared to the other two systems. Trends in the P-P bond length are straightforward and follow the sheet thickness trend, decreasing across the family from Mn to Ni. The 4% drop in the Ni compound creates a “pinch point,” which leads to additional sheet corrugation. The P-S bonds also decrease systematically across the series by about 3.5%, although the difference is largest between the Mn and Fe analogs. In general, the M-S bonds also get shorter in the Mn to Ni series. The overall difference is on the order of 3%, although there are slight variations.  $NiPS_3$  is a special case. Here, the M-S distances are nearly identical. In fact, bond length variations are on the order of only 0.024%. This is consistent with a high-symmetry state (especially compared to  $kT$ ) and suggests that  $NiPS_3$  might be  $P\bar{3}1m$  (or very close to  $P\bar{3}1m$ ) all along rather than  $C2/m$  as suggested by x-ray diffraction work [48–50]. That the  $C_3$  symmetry element is located at the metal center is in line with this supposition as distance (and angle) variations surrounding the metal site are very small. This finding is also consistent with the lack of a  $B_u$  mode signature in the bulk single crystal [Figs. 2(c) and S2] or in any of the sheets. That bond distances are overall longer in  $MnPS_3$  compared to  $NiPS_3$  is consistent with greater ionic (and less covalent) character to the bonds.

Angular trends also impact the symmetry in the  $MPS_3$  family of materials. Overall, the S-P-S angles are very similar, and the differences between these angles get smaller as we go across the Mn to Fe to Ni series. This is consistent with more  $C_3$ -ness and higher-order symmetry. Such a trend would, again, tend to suppress the  $B_u$  vibrational mode. The S-M-S angle is different. It increases across the  $MnPS_3$  to  $NiPS_3$  series, and because changes in this angle move the metal center inward, the overall effect is to increase corrugation. Not only do differences in the S-M-S angle increase across the series, but this angle also differentiates  $MnPS_3$  from  $FePS_3$ . Angular effects may also explain why  $NiPS_3$  is unable to stabilize a magnetic ground state in monolayer form [13].

A full table of bond lengths and angles is provided in the Supplemental Material [16,17,45].

### E. Comparing layer number and pressure effects

Finally, we point out that the space groups preferred by MnPS<sub>3</sub> under confinement are strikingly similar to those under compression. Pressure-induced sliding in MnPS<sub>3</sub> and the Fe analog involves a  $C2/m \rightarrow P\bar{3}1m$  transition [22,25]. Evidence for this crossover is subtle in the phonon response and consists of a slight frequency shift across the critical pressure [25]. The  $A_u + B_u$  modes of MnPS<sub>3</sub>, for instance, are predicted to show a slope change across the  $C2/m \rightarrow P\bar{3}1m$  sliding transition [Fig. 4(d)]. This comparison was carried out by performing both energy and lattice dynamics calculations in the two different phases [25]. Exfoliated MnPS<sub>3</sub> shows a clear frequency shift across the  $C2/m \rightarrow P\bar{3}1m$  transition at  $n = 11$  as well, although the frequencies harden (rather than soften) in few-sheet form [Fig. 4(c)]. The fact that exerting pressure and reducing layer thickness show opposite tendencies is perfectly understandable. The former enhances three-dimensionality, whereas the latter does the opposite. It is more challenging to understand why exerting pressure softens rather than hardens the phonon modes. Here, it is important to realize that frequency vs pressure trends continue to rise but at a slower pace. We speculate that as pressure suppresses the optical band gap [25], enhanced charge fluctuations can be expected to better screen electrostatic potentials, thus softening the phonon modes. Making the sample thinner should reduce layer-normal band dispersion, contributing to a larger optical band gap, reduced charge excitations, and screening, with resulting harder phonon modes. Interestingly, the symmetry of MnPS<sub>3</sub> is predicted to switch back to  $C2/m$  across the pressure-driven insulator-metal transition [25].

These commonalities indicate that the  $C_3$  rotation is a rather fragile symmetry element in the MnPS<sub>3</sub> system, which is indeed the case due to its partially filled  $t_{2g}$  configuration in proximity to its pressure-induced low-spin metallic configuration [25]. On the other hand, the fully occupied  $t_{2g}$  shell in NiPS<sub>3</sub> is consistent with its  $C_3$ -symmetric structure as proposed in this work. Unlike corner-shared geometries such as perovskite structures, partially filled  $e_g$  configurations very weakly couple to the lattice and show almost no Jahn-Teller instability.

## IV. CONCLUSION

To summarize, we employed synchrotron-based near-field infrared nanospectroscopy to explore the symmetry crossover

in the MPS<sub>3</sub> ( $M$ =Mn, Fe, Ni) family of materials in bulk, few-layer, and single-layer form as well as the structure-property relations that can be unraveled in these systems. In MnPS<sub>3</sub>, the  $B_u$  symmetry mode near 450 cm<sup>-1</sup>, which probes the P-P stretch combined with in-phase, out-of-plane PS<sub>3</sub> translation, is exquisitely sensitive to the  $C2/m \rightarrow P\bar{3}1m$  transition that takes place at layer number 11. A similar effect occurs in FePS<sub>3</sub>. The complete loss of the  $B_u$  mode in both materials demonstrates that symmetry is increased in the thinnest sheets. There are also a few subtle differences. In FePS<sub>3</sub>, the  $C2/m \rightarrow P\bar{3}1m$  crossover takes place over a range of thicknesses (rather than at  $n = 11$  as in the Mn compound), and it responds gradually to strain, as evidenced by the systematic frequency shift with decreasing layer number (different from MnPS<sub>3</sub>, which is fairly rigid as the crossover is approached). Strikingly, the third member of this family of materials, NiPS<sub>3</sub>, does not show a symmetry crossover with decreasing sheet thickness. This is because NiPS<sub>3</sub> already exists as  $P\bar{3}1m$  (or very close to  $P\bar{3}1m$ ) in bulk form, at least at room temperature, due to the lack of a clear  $B_u$  symmetry vibrational mode in the spectroscopic response. We analyzed these effects in terms of the stronger interlayer interactions present in the Ni system as well as the local structure within the layer itself. Taken together, we found that monoclinicity in this family of materials is a consequence of long-range stacking, temperature effects, and local lattice distortions. We also compared layer number and pressure trends and note that similar symmetry crossovers are preferred under both confinement and external stimuli.

## ACKNOWLEDGMENTS

Research at the University of Tennessee is supported by the U.S. Department of Energy, Office of Basic Energy Sciences, Materials Science Division under Award No. DE-FG02-01ER45885 (J.L.M.). Work at Rutgers University is funded by the National Science Foundation DMREF program (Grant No. DMR-1629059). D.G.M. acknowledges support from the Gordon and Betty Moore Foundations EPIQS Initiative through Grant No. GBMF9069. A.V.H. acknowledges funding from the Center for Materials Processing, a Tennessee Higher Education Commission (THEC) supported Accomplished Center of Excellence, for funding the crystal synthesis work that provided materials for this research. Portions of these measurements utilized beamline 2.4 at the Advanced Light Source, which is a DOE Office of Science User Facility operated under Contract No. DE-AC02-05CH11231, including the remote user program from NSLS-II under Contract No. DE-SC0012704.

- 
- [1] L. D. Casto, A. J. Clune, M. O. Yokosuk, J. L. Musfeldt, T. J. Williams, H. L. Zhuang, M. W. Lin, K. Xiao, R. G. Hennig, B. C. Sales, J. Q. Yan, and D. Mandrus, *APL Mater.* **3**, 041515 (2015).  
 [2] H. Yang, S. W. Kim, M. Chhowalla, and Y. H. Lee, *Nat. Phys.* **13**, 931 (2017).

- [3] S. Li, Z. Ye, X. Luo, G. Ye, H. H. Kim, B. Yang, S. Tian, C. Li, H. Lei, A. W. Tsen, K. Sun, R. He, and L. Zhao, *Phys. Rev. X* **10**, 011075 (2020).  
 [4] I. Lee, F. G. Utermohlen, D. Weber, K. Hwang, C. Zhang, J. van Tol, J. E. Goldberger, N. Trivedi, and P. C. Hammel, *Phys. Rev. Lett.* **124**, 017201 (2020).

- [5] A. B. Kaul, *J. Mater. Res.* **29**, 348 (2014).
- [6] X. Zhang, X.-F. Qiao, W. Shi, J.-B. Wu, D.-S. Jiang, and P.-H. Tan, *Chem. Soc. Rev.* **44**, 2757 (2015).
- [7] C. T. Kuo, M. Neumann, K. Balamurugan, H. J. Park, S. Kang, H. W. Shiu, J. H. Kang, B. H. Hong, M. Han, T. W. Noh, and J. G. Park, *Sci. Rep.* **6**, 20904 (2016).
- [8] J. U. Lee, S. Lee, J. H. Ryoo, S. Kang, T. Y. Kim, P. Kim, C. H. Park, J.-G. Park, and H. Cheong, *Nano Lett.* **16**, 7433 (2016).
- [9] B. Huang, G. Clark, E. Navarro-Moratalla, D. R. Klein, R. Cheng, K. L. Seyler, D. Zhong, E. Schmidgall, M. A. McGuire, D. H. Cobden, W. Yao, D. Xiao, P. Jarillo-Herrero, and X. Xu, *Nature (London)* **546**, 270 (2017).
- [10] G. Long, T. Zhang, X. Cai, J. Hu, C. W. Cho, S. Xu, J. Shen, Z. Wu, T. Han, J. Lin, J. Wang, Y. Cai, R. Lortz, Z. Mao, and N. Wang, *ACS Nano* **11**, 11330 (2017).
- [11] L. Zhong, X. Chen, and J. Qi, *Phys. Chem. Chem. Phys.* **19**, 15388 (2017).
- [12] Y.-J. Sun, Q.-H. Tan, X.-L. Liu, Y.-F. Gao, and J. Zhang, *J. Phys. Chem. Lett.* **10**, 3087 (2019).
- [13] K. Kim, S. Y. Lim, J. U. Lee, S. Lee, T. Y. Kim, K. Park, G. S. Jeon, C. H. Park, J. G. Park, and H. Cheong, *Nat. Commun.* **10**, 345 (2019).
- [14] P. A. Joy and S. Vasudevan, *J. Phys. Chem. Solids* **54**, 343 (1993).
- [15] Y. Mathey, R. Clement, C. Sourisseau, and G. Lucazeau, *Inorg. Chem.* **19**, 2773 (1980).
- [16] G. Ouvrard, R. Brec, and J. Rouxel, *Mater. Res. Bull.* **20**, 1181 (1985).
- [17] W. Klingen, G. Eulenberger, and H. Hanh, *J. Inorg. Gen. Chem.* **401**, 97 (1973).
- [18] E. Ressouche, M. Loire, V. Simonet, R. Ballou, A. Stunault, and A. Wildes, *Phys. Rev. B* **82**, 100408(R) (2010).
- [19] K. Z. Du, X. Z. Wang, Y. Liu, P. Hu, M. I. B. Utama, C. K. Gan, Q. Xiong, and C. Kloc, *ACS Nano* **10**, 1738 (2016).
- [20] H. Chu, C. J. Roh, J. O. Island, C. Li, S. Lee, J. Chen, J. G. Park, A. F. Young, J. S. Lee, and D. Hsieh, *Phys. Rev. Lett.* **124**, 27601 (2020).
- [21] N. Sivadas, S. Okamoto, and D. Xiao, *Phys. Rev. Lett.* **117**, 267203 (2016).
- [22] C. R. S. Haines, M. J. Coak, A. R. Wildes, G. I. Lampronti, C. Liu, P. Nahai-Williamson, H. Hamidov, D. Daisenberger, and S. S. Saxena, *Phys. Rev. Lett.* **121**, 266801 (2018).
- [23] F. Wang, T. A. Shifa, P. Yu, P. He, Y. Liu, F. Wang, Z. Wang, X. Zhan, X. Lou, F. Xia, and J. He, *Adv. Funct. Mater.* **28**, 1802151 (2018).
- [24] C. M. Pasco, I. El Baggari, E. Bianco, L. F. Kourkoutis, and T. M. McQueen, *ACS Nano* **13**, 9457 (2019).
- [25] N. Harms, H.-S. Kim, A. J. Clune, K. Smith, K. R. O'Neal, A. Haglund, D. G. Mandrus, Z. Liu, K. Haule, D. Vanderbilt, and J. L. Musfeldt, *npj Quantum Materials* (to be published).
- [26] K. Kyriazi and J. Singleton (unpublished).
- [27] H. Li, Q. Zhang, C. C. R. Yap, B. K. Tay, T. H. T. Edwin, A. Olivier, and D. Baillargeat, *Adv. Funct. Mater.* **22**, 1385 (2012).
- [28] J. Lee, T. Y. Ko, J. H. Kim, H. Bark, B. Kang, S. G. Jung, T. Park, Z. Lee, S. Ryu, and C. Lee, *ACS Nano* **11**, 10935 (2017).
- [29] H. A. Bechtel, E. A. Muller, R. L. Olmon, M. C. Martin, and M. B. Raschke, *Proc. Natl. Acad. Sci. USA* **111**, 7191 (2014).
- [30] E. A. Muller, B. Pollard, and M. B. Raschke, *J. Phys. Chem. Lett.* **6**, 1275 (2015).
- [31] M. Hafeez, L. Gan, H. Li, Y. Ma, and T. Zhai, *Adv. Funct. Mater.* **26**, 4551 (2016).
- [32] A. Alkabsh, H. Samassekou, and D. Mazumdar, *Nanotechnology* **30**, 03LT02 (2019).
- [33] M. Patel, J. Kim, and Y. K. Kim, *Adv. Funct. Mater.* **28**, 1804737 (2018).
- [34] Y. R. Sapkota and D. Mazumdar, *J. Appl. Phys.* **124**, 105306 (2018).
- [35] J. Chen, M. Badioli, P. Alonso-González, S. Thongrattanasiri, F. Huth, J. Osmond, M. Spasnović, A. Centeno, A. Pesquera, P. Godignon, A. Zurutuza Elorza, N. Camara, F. J. G. de Abajo, R. Hillenbrand, and F. H. L. Koppens, *Nature (London)* **487**, 77 (2012).
- [36] S. N. Neal, H.-S. Kim, K. A. Smith, A. V. Haglund, D. G. Mandrus, H. A. Bechtel, G. L. Carr, K. Haule, D. Vanderbilt, and J. L. Musfeldt, *Phys. Rev. B* **100**, 075428 (2019).
- [37] K. A. Smith, E. A. Nowadnick, S. Fan, O. Khatib, S. J. Lim, B. Gao, N. C. Harms, S. N. Neal, J. K. Kirkland, M. C. Martin, C. J. Won, M. B. Raschke, S. W. Cheong, C. J. Fennie, G. L. Carr, H. A. Bechtel, and J. L. Musfeldt, *Nat. Commun.* **10**, 5235 (2019).
- [38] R. Nitsche and P. Wild, *Mater. Res. Bull.* **5**, 419 (1970).
- [39] O. Khatib, H. A. Bechtel, M. C. Martin, M. B. Raschke, and G. L. Carr, *ACS Photonics* **5**, 2773 (2018).
- [40] G. Kresse and J. Furthmüller, *Phys. Rev. B* **54**, 11169 (1996).
- [41] G. Kresse and D. Joubert, *Phys. Rev. B* **59**, 1758 (1999).
- [42] J. P. Perdew, A. Ruzsinszky, G. I. Csonka, O. A. Vydrov, G. E. Scuseria, L. A. Constantin, X. Zhou, and K. Burke, *Phys. Rev. Lett.* **100**, 136406 (2008).
- [43] S. L. Dudarev, G. A. Botton, S. Y. Savrasov, C. J. Humphreys, and A. P. Sutton, *Phys. Rev. B* **57**, 1505 (1998).
- [44] A. Togo and I. Tanaka, *Scr. Mater.* **108**, 1 (2015).
- [45] See Supplemental Material at <http://link.aps.org/supplemental/10.1103/PhysRevB.102.085408> for traditional infrared and Raman spectra, tables with displacement patterns and bond lengths and angles, a detailed analysis of the  $B_u$  mode in the single crystal, and a discussion on the signal-to-noise ratio in the near-field infrared response of atomically thin materials.
- [46] E. Pensa, E. Cortés, G. Corthey, P. Carro, C. Vericat, M. H. Fonticelli, G. Benítez, A. A. Rubert, and R. C. Salvarezza, *Acc. Chem. Res.* **45**, 1183 (2012).
- [47] These thermal fluctuations are not an effect of the incident light but rather of room temperature.
- [48] N. Ismail, Y. M. Temerk, A. A. El-Meligi, M. A. Badr, and M. Madian, *J. Solid State Chem.* **183**, 984 (2010).
- [49] R. N. Jenjeti, R. Kumar, M. P. Austeria, and S. Sampath, *Sci. Rep.* **8**, 8586 (2018).
- [50] Z. Ur Rehman, Z. Muhammad, O. A. Moses, W. Zhu, C. Wu, Q. He, M. Habib, and L. Song, *Micromachines* **9**, 292 (2018).
- [51] A. R. Wildes, V. Simonet, E. Ressouche, G. J. McIntyre, M. Avdeev, E. Suard, S. A. J. Kimber, D. Lançon, G. Pepe, B. Moubaraki, and T. J. Hicks, *Phys. Rev. B* **92**, 224408 (2015).